DINAME 2017 - Proceedings of the XVII International Symposium on Dynamic Problems of Mechanics
A. T. Fleury, D. A. Rade, P. R. G. Kurka (Editors), ABCM, São Sebastião, SP, Brazil, March 5-10, 2017

Cable Dynamic Modeling and Applications

Sebastião C. P. Gomes, Elisane B. Zanela, Adriana E. L. Pereira

Universidade Federal do Rio Grande, Instituto de Matemática, Estatística e Física
Avenida Itália, km 8, 96201-900, Rio Grande, RS
sebastiaogomes@furg.br, laplaciano2000@bol.com.br, adrianapereira@furg.br

Abstract: Dynamic modeling of cables in three-dimensional space is a problem with great difficulty and complexity. This article discusses a new dynamic modeling formalism, including applications in the underwater environment. It is assumed that the cable is formed by rigid links connected by elastic fictitious joints, allowing elevation, azimuth and torsion movements. Algorithms have been developed to automatically generate the dynamic model for any number of links selected for the discrete approximation of the flexible structure. Two practical situations are tested: cable with free terminal load considering dynamics with or without ocean current. Simulations showed results physically expected and three-dimensional animations attested a great sense of physical reality.

Keywords: cable, dynamic, modeling, algorithms, automatic generation model, underwater applications.

INTRODUCTION

Cable dynamic modeling is a complicated task because of its complexity, especially in the case of movement in three dimensional space. Many applications involving cable dynamics occur in the underwater environment: risers, mooring lines, towing cables, etc., can be examples of offshore oil industry applications (see Fig. 1).

Most studies found in the literature address the modeling of these structures using Finite Element Methods (Wang *et al*., 1998; Gosling and Korban, 2001). Other authors also used finite element methods for the structural dynamic analysis of flexible cables (Buckam *et al*., 2004; Srinil *et al*, 2007; Yoon *et al*., 2008). Sun *et al*. (2011) introduced a finite element method to modeling a cable towed body.

Some authors have developed their works performing a cable static analysis (Hover *et al*., 1994; Matulea *et al*., 2008; Wang *et al*. 2008), using the method of finite differences. A static analysis of two-dimensional cables is also made in Dreyer and Van Vuuren (1999), using numerical solution of both continuous and discrete models. Discrete approach was used specially in static analysis: Raman-Nair *et al*. (2005) have used a discrete model to reproduce structural forces acting into a flexible marine riser under effects of flow and pressure of fluid within the riser; Zhu *et al.* (2008) proposed a discrete model to determine the forces that an umbilical cable exerts on a ROV (Remotely Operated Vehicle).

When the discrete formalism is used in dynamic modeling, usually lumped mass approach is applied, considering the dynamics evolving in a single plane. A simulation of cable dynamics for kities was made by Breukels and Ockels (2007) considering each link with one degree of freedom mass spring damper model and in that case, the flexible structure's motion was restricted in a single vertical plane. Hall and Goupee (2015) used a lumped mass approach to model a mooring line and validated the simulations with an offshore wind turbine test data.

Finite differences are widely used in cable modeling. Lacarbonara and Pacitti (2008) used finite differences to model cables suffering axis stretching and flexural curvature. In Srivastava *et al*. (2011) a three-dimensional model of underwater towed cable was studied and governing equations were solved using a central finite-difference method. Matulea *et al*. (2014) used finite differences to determine the static equilibrium configuration of the riser, and then to find its dynamic response around the formerly computed static configuration, considering the flexible structure restrict to the vertical plane. Lee *et al*. (2015) applied finite difference method with lumped mass to model a flexible pipe. Zhang and Li (2015) analyzed axial dynamic stress response of deep water risers and a Linear Quadratic Gaussian control was proposed to deal with this problem.

In short, most of the articles that deal with cables treat the problem as restricted to a single plane using finite elements or finite differences for the dynamic model. Other works focus interest in static analysis of axial forces on the cable. Gobat (2000) in his thesis provides details about these main methods used in cable dynamics.

This paper introduces a new method to automatically obtain vectors and matrices elements of a cable dynamic model. We use a discrete formalism to represent the continuous flexibility from a chain of rigid links connected by fictitious elastic joints. Each joint allows three elastic movements: elevation, azimuth and torsion. We take as a basis the work of Gomes *et al.* 2006, where a discrete formalism was used to model a robotic manipulator with a single flexible link. In that case, the flexibility occurred on a single plane and each joint had one degree of freedom. Based on this

work, Pereira *et al.* (2012) developed the analytical modeling of a cable considering three links, but with spatial flexibility, i.e. the discrete formalism was used without the motion being restricted to a single plane. In Gomes *et al.* (2016) algorithms were presented to automatically generate the dynamic model, for any number of links to be used in discrete approximation of the continuous cable flexibility. The present article shows this theory in two possible underwater applications, considering underwater currents acting as external efforts. Automatic retrieval models are very important due to the great complexity of the equations that turn unfeasible obtain these models manually through the application of the Euler-Lagrange equations.

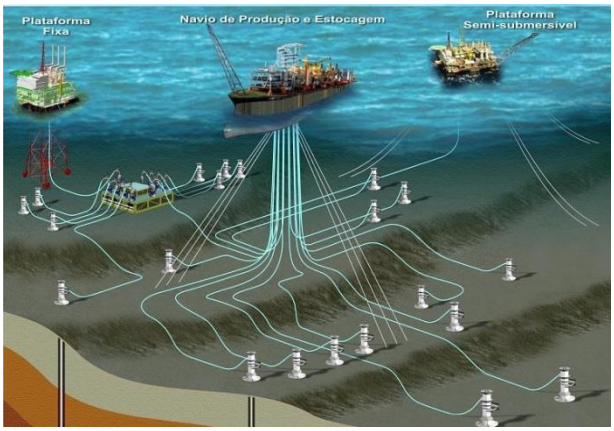

Fig. 1 Floating system of oil production (source: http://diariodopresal.wordpress.com/petroleo-e-gas).

DYNAMIC MODELING

In this work it is considered a cylindrical cable with constant radius, fixed at one extremity (fixed base) and free at the other, where there is a terminal load m_c. The basic principle of this modeling theory is to approximate the continuous flexibility by a discrete equivalent one, consisting of rigid links connected by flexible fictitious joints, as showed in Fig. 2. Each fictitious elastic joint allows three movements: elevation (θ_{ie}), azimuth (θ_{ia}) and torsion (θ_{iT}), $i = 1, \dots, n$. Therefore, this dynamic system has $3n$ degrees of freedom when considering n links. In each fictitious joint is positioned a reference frame, as shown in Fig. 3 for the first two systems. The first is an inertial system ($X_0\ Y_0\ Z_0$). It was adopted the following convention for reference systems: all Z axes point to the center of the Earth and thus, the XY axes form horizontal planes. The Y_i axes are parallel to the projection of the link i on the $X_{i-1}Y_{i-1}$ plane, as showed in Figures 3 and 4. For instance, Y_1 is parallel to r in Fig. 3. Fig. 4 also shows the three angular positions coordinates of the first joint and the three others of the second fictitious joint. As all links are rigid, torsion motions are considered as rotations about the longitudinal axis of the links.

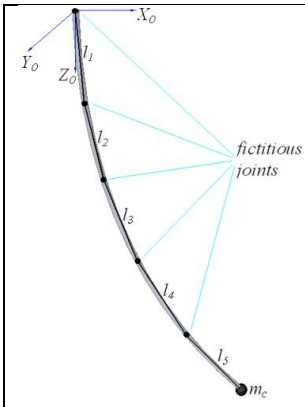

Fig.2 Continuous flexibility and its discrete approximation.

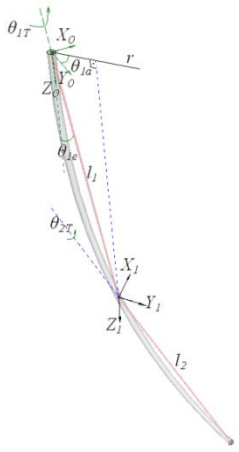

Fig. 3 Angular coordinates of the first joint.

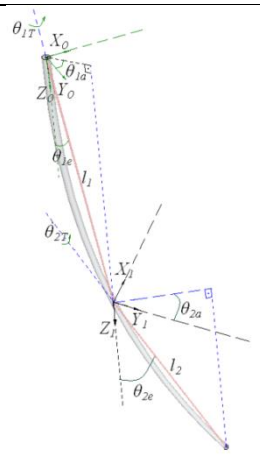

Fig. 4 The first two reference systems and its angular coordinates.

It is simple to find a homogeneous transformation matrix between two consecutive reference systems. For example, the homogeneous matrix that relates $X_0Y_0Z_0$ and $X_1Y_1Z_1$ systems has the form:

$$H_{01}=\begin{bmatrix} \cos\theta_{1a} & \sin\theta_{1a} & 0 & l_1\sin\theta_{1e}\sin\theta_{1a} \\ -\sin\theta_{1a} & \cos\theta_{1a} & 0 & l_1\sin\theta_{1e}\cos\theta_{1a} \\ 0 & 0 & 1 & l_1\cos\theta_{1e} \\ 0 & 0 & 0 & 1 \end{bmatrix} \tag{1}$$

The products between successive homogeneous matrices generate another homogeneous matrix that can relate any mobile reference system to the base inertial system of the structure. Thus, the spatial position of the center of mass of any link in the inertial frame may be determined as functions of the lengths of the links and the angular position coordinates, as specified below $(k=1,\ldots,n)$:

$$\begin{cases} x_k = \dfrac{l_k}{2}\sin\theta_{ke}\sin\left(\displaystyle\sum_{i=1}^{k}\theta_{ia}\right)+\displaystyle\sum_{j=1}^{k-1}\left[l_j\sin\theta_{je}\sin\left(\displaystyle\sum_{i=1}^{j}\theta_{ia}\right)\right] \\ y_k = \dfrac{l_k}{2}\sin\theta_{ke}\cos\left(\displaystyle\sum_{i=1}^{k}\theta_{ia}\right)+\displaystyle\sum_{j=1}^{k-1}\left[l_j\sin\theta_{je}\cos\left(\displaystyle\sum_{i=1}^{j}\theta_{ia}\right)\right] \\ z_k = \dfrac{l_k}{2}\cos\theta_{ke}+\displaystyle\sum_{j=1}^{k-1}l_j\cos\theta_{je} \end{cases} \tag{2}$$

Arising from the same formalism, spatial coordinates of the terminal load (written in the inertial frame) have the form:

$$\begin{cases} x_c = \displaystyle\sum_{j=1}^{n}\left[l_j\sin\theta_{je}\sin\left(\displaystyle\sum_{i=1}^{j}\theta_{ia}\right)\right] \\ y_c = \displaystyle\sum_{j=1}^{n}\left[l_j\sin\theta_{je}\cos\left(\displaystyle\sum_{i=1}^{j}\theta_{ia}\right)\right] \\ z_c = \displaystyle\sum_{j=1}^{n}l_j\cos\theta_{je} \end{cases} \tag{3}$$

The time derivatives of the equations (2) and (3) can be easily obtained and thus the Lagrangian of the system can be obtained only as function of the angular position and velocity coordinates (see Gomes *et al*., (2016) for more details). Each new link considered in the discrete approach means three degrees of freedom more in the model. Thus, when *n* links are considered, the dynamic model will have 3*n* degrees of freedom. The application of the 3*n* Euler-Lagrange equations allows finding the dynamic model in the form:

$$I(\vec{\theta})\ddot{\vec{\theta}} + C\dot{\vec{\theta}} + K\vec{\theta} + \vec{f}\left(\vec{\theta},\dot{\vec{\theta}}\right) + \vec{G}(\vec{\theta}) = \vec{\tau} \tag{4}$$

where $\vec{\theta} = [\theta_{1e}\ \theta_{2e}\ \ldots\ \theta_{ne}\ \theta_{1a}\ \theta_{2a}\ \ldots\ \theta_{na}\ \theta_{1T}\ \theta_{1T}\ \ldots\ \theta_{nT}]^T$ is the angular position vector, θ_{ie}, θ_{ia} and θ_{iT} are elevation, azimuth and torsion angles of the link i $(i = 1, \ldots, n)$, $I(\vec{\theta})$ is the inertia matrix, C is the friction coefficient matrix, K is the elastic constant matrix, $\vec{f}\left(\vec{\theta},\dot{\vec{\theta}}\right)$ is the Coriolis-centrifugal vector, $\vec{G}(\vec{\theta})$ is the gravitational vector and $\vec{\tau}$ is the external torques vector. All matrices are (3*n* x 3*n*) and vectors are (3*n* x 1). It is important to explain that the matrices of the friction coefficients and elastic constants have the same configuration and also, all matrices of the dynamic models are symmetric.

GENERIC ALGORITHM

Equation (4) was manually developed considering 1, 2, 3 and 4 links and so it was possible to identify growth patterns for matrices and vectors of the dynamic model, shown below in the form of algorithms that can automatically generate the vectors and matrices of the model, for any adopted number of links.

Algorithms for the Elements of Inertia Matrix

To facilitate understanding, the inertia matrix *I* is represented through nine submatrices, as indicated below, where indices *e*, *a* and *t* mean elevation, azimuth and torsion, respectively.

$$I = \begin{bmatrix} I_e & N_e & T_e \\ I_a & N_a & T_a \\ I_t & N_t & T_t \end{bmatrix} \tag{5}$$

I is symmetric and thus, $I_a = N_e^T$; $I_t = T_e^T$; $N_t = T_a^T$. As there is a dynamic decoupling of the torsion movement with

respect to elevation and azimuth motions, submatrices T_e and T_a are null and T_t is diagonal. Elements of T_t are constant and equivalent to $I_{iT} = (m_i/2)r_i^2$, where m_i and r_i are mass and radius of the link i, respectively, with $i = 1, \dots, n$. Due to the symmetry of the inertia matrix the interest is to determine the rules for the automatic generation of I_e, N_e and N_a.
The submatrix I_e can be generated from the following algorithm:

$$
\begin{aligned}
&for\ i = 1{:}n,\\
&\quad for\ j = i+1{:}n,\\
&\qquad I_e(i,j) = l_i l_j \left(\frac{m_j}{2} + m_c + \sum_{k=j+1}^{n} m_k\right)\left[\cos\theta_{ie}\cos\theta_{je}\cos\left(\sum_{k=i+1}^{j}\theta_{ka}\right) + sin\,\theta_{ie}\,sin\,\theta_{je}\right];\\
&\quad end,\\
&\quad I_e(i,i) = l_i^2\left[\frac{m_i}{4} + m_c + \sum_{k=i+1}^{n}(m_k)\right] + I_{ie};\\
&end,
\end{aligned}
\tag{6}
$$

As I_e is symmetric, $I_e(j,i) = I_e(i,j)$. I_{ie} is the elevation rotational inertia moment of the link i.
The submatrix N_e can be generated from the following algorithm:

$$
\begin{aligned}
&for\ i = 1{:}n,\\
&\ for\ j = 1{:}n,\\
&\quad if\ i \neq j,\\
&\qquad S = 0;\\
&\qquad for\ k = j{:}n,\\
&\qquad\ if\ k \neq i,\\
&\qquad\quad if\ i > k,\ \mu = 1;\ \alpha = i;\ else\ \ \mu = -1;\ \alpha = k;\ \ endif,\\
&\qquad\quad v = [i\quad k];\\
&\qquad\quad S = S + \mu l_k\left[\frac{m_\alpha}{2} + m_c + \sum_{g=max(v)+1}^{n} m_g\right]cos(\theta_{ie})sin(\theta_{ke})sin\left(\sum_{g=min(v)+1}^{max(v)}\theta_{ga}\right);\\
&\qquad\ endif,\\
&\qquad end,\\
&\qquad N_e(i,j) = l_i S;\\
&\quad endif,\\
&\ end,\\
&end,\\
&for\ i = 1{:}n-1,\\
&\ N_e(i,i) = N_e(i,i+1);\\
&end,\\
&N_e(n,n) = 0;
\end{aligned}
\tag{7}
$$

The submatrix N_a can be generated from the following algorithm:

$$
\begin{aligned}
&for\ i = 1{:}n,\\
&\ for\ j = i{:}n,\\
&\quad S_1 = 0;\\
&\quad for\ k = j{:}n,\\
&\qquad S_1 = S_1 + l_k^2\left[\frac{m_k}{4} + m_c + \sum_{h=k+1}^{n} m_h\right]sin^2(\theta_{ke});\\
&\quad end,\\
&\quad S_2 = 0;\\
&\quad v = [i\ \ j];\\
&\quad for\ k = min(v){:}n-1,\\
&\qquad S_3 = 0;\\
&\qquad for\ g = j{:}n,\\
&\qquad\ if\ g > k,\\
&\qquad\quad \sigma = 1;\\
&\qquad\quad if\ (i = 1\ and\ j = 1)\ or\ k \geq j,\\
&\qquad\qquad \sigma = 2;
\end{aligned}
\tag{8}
$$

$$
\begin{aligned}
&\quad endif,\\
&\quad S_3 = S_3 + \sigma l_g \left[\frac{m_g}{2} + m_c + \sum_{h=g+1}^{n} m_h\right] sin(\theta_{ke}) sin(\theta_{ge}) cos\left(\sum_{h=k+1}^{g} \theta_{ha}\right);\\
&\quad endif,\\
&\quad end,\\
&\quad S_2 = S_2 + l_k S_3;\\
&\quad end,\\
&\quad if\ (i = n)\ and\ (j = n),\\
&\quad\quad S_2 = 0;\\
&\quad endif,\\
&\quad N_a(i,j) = S_1 + S_2;\\
&\quad N_a(j,i) = N_a(i,j);\\
&\quad if\ i = j,\\
&\quad\quad N_a(i,i) = N_a(i,i) + I_{ia};\\
&\quad endif,\\
&\quad end,\\
&end,
\end{aligned}
$$

I_{ia} is the azimuth rotational inertia moment of the link *i*.

Algorithms for the Elements of Coriolis-Centrifugal Vector

The first *n* elements of the Coriolis-centrifugal vector are related to the elevation motion, the intermediate *n* are related to the azimuthal motion and the last *n* elements are null (torsion motion).
Coriolis-centrifugal vector can be written as:

$$\vec{f}\left(\vec{\theta}, \dot{\vec{\theta}}\right) = [f_1\ \ f_2\ \ \dots\ \ f_n\ \ f_{n+1}\ \ f_{n+2}\ \dots\ f_{2n}\ \ f_{2n+1}\ \ f_{2n+2}\ \dots\ f_{3n}]^T \tag{9}$$

Elements of elevation are $[f_1\ \ f_2\ \ \dots\ \ f_n]^T$, f_i, $(i = 1, \dots, n)$, and can be obtained from the following algorithm:

$$f_i = \vartheta_1 + \vartheta_2 \tag{10}$$

$$\vartheta_1 = \alpha l_i^2 \left[\frac{m_i}{4} + m_c + \sum_{g=i+1}^{n} m_g\right] sin(\theta_{ie}) cos(\theta_{ie}) \left\{\left[\sum_{g=1}^{i-1}\left(\dot{\theta}_{ga} \sum_{h=g+1}^{i} \dot{\theta}_{ha}\right)\right] + \frac{1}{|\alpha|}\left(\sum_{g=1}^{i} \dot{\theta}_{ga}^2\right)\right\} \tag{11}$$

$$\alpha = \begin{cases} -1 & for\ i = 1;\\ -2 & for\ i \neq 1; \end{cases} \tag{12}$$

$$
\begin{aligned}
\vartheta_2 = l_i \sum_{\substack{j=1\\ j\neq i}}^{n} \Bigg\{ & \beta l_j \left(\frac{m_{\max(i,j)}}{2} + m_c \right.\\
& \left. + \sum_{g=\max(i,j)+1}^{n} m_g\right)\Bigg[cos(\theta_{ie})\Bigg[cos(\theta_{je}) sin\left(\sum_{g=\min(i,j)+1}^{\max(i,j)} \theta_{ga}\right)\dot{\theta}_{je}\left(\sum_{g=1}^{j} \dot{\theta}_{ga}\right)\\
& - sign(\beta)\left(sin(\theta_{je}) cos\left(\sum_{g=\min(i,j)+1}^{\max(i,j)} \theta_{ga}\right)\left(\sum_{g=1}^{j-1}\left(\dot{\theta}_{ga} \sum_{h=g+1}^{j} \dot{\theta}_{ha}\right)\right.\right.\\
& \left.\left. + \frac{1}{2}\left(\dot{\theta}_{je}^2 + \sum_{g=1}^{j} \dot{\theta}_{ga}^2\right)\right)\right)\Bigg] + \frac{1}{\beta} sin(\theta_{ie}) cos(\theta_{je}) \dot{\theta}_{je}^2\Bigg]\Bigg\}
\end{aligned}
\tag{13}
$$

$$\beta = \begin{cases} 2 & for\ \ i > j,\\ -2 & for\ \ i \leq j \end{cases} \tag{14}$$

Azimuth elements of the Coriolis-centrifugal vector are defined as $z_i = f_{n+i}$ and then:

$$\vec{Z} = [f_{n+1}\ \ f_{n+2}\ \dots\ f_{2n}]^T = [z_1\ \ z_2\ \dots\ z_n]^T \tag{15}$$

We can define vector $\vec{Z}$ as:

$$\vec{Z} = \vec{R} + W\vec{P} \tag{16}$$

W is a (n x q) matrix, $\vec{R}$ is (n x 1) and $\vec{P}$ is (q x 1), where $q = q(n) = q_n$ is obtained through the sequence function of n:

$$q_1 = 0;\ \ q_i = q_{i-1} + i - 1;\ \ i = 2,3,\dots n \tag{17}$$

Elements of vector $\vec{R}$ are defined as $(i = 1, \dots, n)$:

$$R_i = 2\sum_{k=i}^{n}\left\{ l_k^2\left(\frac{m_k}{4} + m_c + \sum_{g=k+1}^{n} m_g\right) sin(\theta_{ke}) cos(\theta_{ke}) \left(\sum_{g=1}^{k} \dot{\theta}_{ga}\right)\dot{\theta}_{ke}\right\} \tag{18}$$

P_u elements of $\vec{P}$ vector has the following definition:

$$\begin{aligned}
&u = 0;\\
&for\ i = 1{:}n,\\
&\quad for\ j = i+1{:}n,\\
&\quad\quad u = u + 1;\\
&\quad\quad P_u = 2l_i l_j\left[\frac{m_j}{2} + m_c + \sum_{g=j+1}^{n} m_g\right];\\
&\quad end,\\
&end,
\end{aligned} \tag{19}$$

W matrix has the form:

$$W = \begin{bmatrix} w_{11} & \cdots & w_{1q} \\ \vdots & \ddots & \vdots \\ w_{n1} & \cdots & w_{nq} \end{bmatrix} \tag{20}$$

Elements of the W matrix are defined as:

$$w_{k,u} = a_{k,u} + b_{k,u} + c_{k,u} \tag{21}$$

$a_{k,u}$, $b_{k,u}$ and $c_{k,u}$ can be generated from the following algorithm:

$$\begin{aligned}
&for\ k = 1{:}n,\\
&\quad u = 0;\\
&\quad for\ i = 1{:}n-1,\\
&\quad\quad for\ j = i+1{:}n,\\
&\quad\quad\quad u = u + 1;\\
&\quad\quad\quad if\ j \geq k,\\
&\quad\quad\quad\quad if\ i < k,\\
&\quad\quad\quad\quad\quad c_{k,u} = sin(\theta_{ie}) sin(\theta_{je}) sin\left(\sum_{g=i+1}^{j}\theta_{ga}\right)\varphi_1\left(\dot{\vec{\theta}}_e, \dot{\vec{\theta}}_a, i, j\right);\\
&\quad\quad\quad\quad else\\
&\quad\quad\quad\quad\quad c_{k,u} = sin(\theta_{ie}) sin(\theta_{je}) sin\left(\sum_{g=i+1}^{j}\theta_{ga}\right)\varphi_2\left(\dot{\vec{\theta}}_e, \dot{\vec{\theta}}_a, i, j\right);\\
&\quad\quad\quad\quad endif,\\
&\quad\quad\quad else\\
&\quad\quad\quad\quad c_{k,u} = 0;\\
&\quad\quad\quad endif,\\
&\quad\quad\quad if\ (k = 1)\ or\ (k \geq 2)\ and\ (k < n)\ and\ (i \geq k),\\
&\quad\quad\quad\quad b_{k,u} = sin(\theta_{ie}) cos(\theta_{je}) cos\left(\sum_{g=i+1}^{j}\theta_{ga}\right)\left[\left(\sum_{g=1}^{j}\dot{\theta}_{ga}\right)\dot{\theta}_{je}\right];\\
&\quad\quad\quad else\\
&\quad\quad\quad\quad b_{k,u} = 0;
\end{aligned} \tag{22}$$

$$
\begin{array}{l}
\quad endif, \\
\quad if\ j > k, \\
\qquad\qquad a_{k,u} = cos(\theta_{ie}) sin(\theta_{je}) cos\left(\sum_{g=i+1}^{j} \theta_{ga}\right)\left[\left(\sum_{g=1}^{i} \dot{\theta}_{ga}\right)\dot{\theta}_{ie}\right]; \\
\quad else \\
\qquad\qquad a_{k,u} = 0; \\
\quad endif, \\
\quad w_{k,u} = a_{k,u} + b_{k,u} + c_{k,u}; \\
\ end, \\
end, \\
end,
\end{array}
$$

There are two different equations for $c_{k,u}$ elements, depending on the functions $\varphi_1\left(\dot{\bar{\theta}}_e, \dot{\bar{\theta}}_a, i, j\right)$ and $\varphi_2\left(\dot{\bar{\theta}}_e, \dot{\bar{\theta}}_a, i, j\right)$, as specified below:

$$\varphi_1\left(\dot{\bar{\theta}}_e, \dot{\bar{\theta}}_a, i, j\right) = \left\{\sum_{g=1}^{i-1}\left(\dot{\theta}_{ga}\sum_{h=g+1}^{i}\dot{\theta}_{ha}\right) + \frac{1}{2}\left[\left(\sum_{g=1}^{i}\dot{\theta}_{ga}^2\right) + \dot{\theta}_{ie}^2\right]\right\} \tag{23}$$

$$\varphi_2\left(\dot{\bar{\theta}}_e, \dot{\bar{\theta}}_a, i, j\right) = -\left\{\sum_{g=1}^{j-1}\left(\dot{\theta}_{ga}\sum_{h=g+1}^{j}\dot{\theta}_{ha}\right) + \frac{1}{2}\left[\left(\sum_{g=i+1}^{j}\dot{\theta}_{ga}^2\right) + \dot{\theta}_{je}^2 - \dot{\theta}_{ie}^2\right]\right\} \tag{24}$$

Gravitational Vector, Friction and Elastic Coefficients Matrix Generation

Observing the equations of the dynamic model for cases 1, 2, 3 and 4 links, one realizes that the generation of the first *n* elements of the gravitational vector obeys the following rule:

$$G_i = l_i\left(\frac{m_i}{2} + \sum_{k=i+1}^{n} m_k\right) g \sin\theta_{ie} \tag{25}$$

with $i = 1, \ldots, n$. The others elements for $i = n+1, \ldots, 3n$ are nulls. Torques caused by buoyancy forces have the same structures as in equation (25), but with a negative sign (gravitational and buoyancy forces acting in opposite senses). As the geometry of the links is known, masses of fluid equivalent to the volume of each link are also known, so that equation (25) can easily be adapted to generate buoyancy torques.

As explained previously, the matrices of friction coefficients and elastic constants have the same generation rule, showed at the following algorithm (for the elastic constants matrix):

$$
\begin{array}{l}
for\ i = 1{:}n,\ \ for\ j = 1{:}n,\ \ k(i,j) = 0;\ \ \ end,\ \ end, \\
\quad for\ i = 1{:}n, \\
\qquad for\ j = 1{:}n, \\
\qquad\quad if\ \ (i = j)\ and\ \ (i < n), \\
\qquad\qquad k(i,j) = k_{ie} + k_{(i+1)e}; \\
\qquad\quad endif, \\
\qquad\quad if\ \ (i = j)\ and\ \ (i = n), \\
\qquad\qquad k(i,j) = k_{ie}; \\
\qquad\quad endif, \\
\qquad\quad if\ j = i + 1, \\
\qquad\qquad k(i,j) = -k_{je}; \\
\qquad\qquad k(j,i) = k(i,j); \\
\qquad\quad endif, \\
\qquad end, \\
\quad end,
\end{array}
\tag{26}
$$

k_{ie} $(i = 1, \ldots, n)$ is the elevation elastic constant of the joint *i*. Algorithm (26) generates the elevation submatrix K_e. An identical rule is used to generate the azimuth submatrix K_a, considering, in this case, the azimuth elastic constant k_{ia} $(i = 1, \ldots, n)$. The same generation rule is also used to the torsion matrix K_T., considering k_{iT} $(i = 1, \ldots, n)$. The complete elastic constant matrix *K* is (3*n* x 3*n*), as well as the friction coefficient matrix *C*, and both are written in the form:

$$K = \begin{bmatrix} K_e & 0 & 0 \\ 0 & K_a & 0 \\ 0 & 0 & K_T \end{bmatrix};\ \ C = \begin{bmatrix} C_e & 0 & 0 \\ 0 & C_a & 0 \\ 0 & 0 & C_T \end{bmatrix} \tag{27}$$

SIMULATION RESULTS

Simulations were performed considering two application situations in the underwater environment. In both situations, the cable has one end fixed to a structure at the water surface. Its other end is free and simulations are performed with or without considering ocean current. The hydrodynamic drag is modeled in a simple way, where the drag force is proportional to the square of the relative velocity between the structure and the water. The following table shows all the physical parameters used to perform the simulations.

Table I. Physical parameters used in simulations.

Parameters	Numerical value	Physical meaning
L_c	$1200(m)$	Cable length
n	32	Number of links
r_i	$0.01(m)$	Radius of each link (constant)
m_e	7850 (kg/m^3)	Cable specific mass
m_c	600 (kg)	Terminal load mass
l_i	$\frac{L_c}{n}\ (m)$	Length of each link
m_i	$\pi r_i^2 l_i m_e\ (kg)$	Mass of each link
I_{ie}	$\frac{m_i}{12} l_i^2 (kgm^2)$	Elevation rotational inertia
I_{ia}	$I_{ie}[(1-\gamma)\lvert sin\theta_{ie}\rvert + \gamma](kgm^2)$	Azimuth rotational inertia
γ	0.1	Dimensionless coeficiente
I_{iT}	$\frac{m_i}{2} r_i^2 (kgm^2)$	Torsion rotational inertia
k_{ie}	$\frac{5}{6}\frac{nEI_{cs}}{L_c}\left(\frac{Nm}{rd}\right)$	Elastic constant of elevation
E	$8e10\ (Nm^2)$	Young's module
I_{cs}	$\frac{1}{4}\pi r_i^4\ (m^4)$	Inertia of the cross section
k_{ia}	Zero	Azimuth elastic constant
k_{iT}	$250K_{ie}\left(\frac{Nm}{rd}\right)$	Torsion elastic constant
c_e	$33n\left(\frac{Nms}{rd}\right)$	Elevation friction coefficient
c_a	$33n\ \left(\frac{Nms}{rd}\right)$	Azimuth friction coefficient
c_t	$0.83n\ \left(\frac{Nms}{rd}\right)$	Torsion friction coefficient
c_v	$800\left(\frac{Ns^2}{m^2}\right)$	Hydrodynamic drag coefficient
E_{ct}	$0.95m_c g\ (N)$	Terminal load buoyancy

The first simulation shows the cable in free fall from an initial spatial configuration in the underwater environment. Fig. 5 shows a sequence of frames with the cable spatial configuration, from zero to 30 *s* every 2 *s*. The cable terminal load appears in red in the animations with the simulation results. As explained before, it was used a simple model for the hydrodynamic drag, proportional to the square of the relative velocity between the fluid and the structure. This external effort was primarily responsible for the slow cable movement in free fall, seen in Fig. 5.

Fig. 6 shows results of a simulation similar to the previous one, but considering the cable out of the water. The frames also are from zero to 30 *s* every 2 *s*. In this case, cable's dynamic is obviously faster. Fig. 7 shows the two cases simultaneously, each with spatial configurations on the same graph. The three-dimensional animations of the spatial configuration of the cable (Fig. 5, 6 and 7) allow showing that the simulation results give a great sense of physical reality.

Fig. 8 shows 22 *s* of simulation with frames every 2 *s*, considering an ocean current acting on the cable with speed of 2.5 *m / s*. Drag forces was considered proportional to the square of the relative velocities between fluid and structure. The cable is initially at rest in its vertical position and with free terminal load. The ocean current starts from zero initial time and then imposes a significant dynamic disturbance to the cable. If the cable terminal load is a remotely operated vehicle (ROV), the ocean current can to induce dynamic disturbances to the cable that would be transmitted to the vehicle, thus hindering the performance of any control strategy.

CONCLUSIONS

Nature follows growth patterns in their phenomena, but we cannot always identify them. The discrete approach proposed in the modeling formalism approximates the real continuous flexibility when increasing the number of links. Each new link considered increases in three degrees of freedom the cable dynamics, and its equations grow considerably in size and complexity. It was possible to identify patterns of this growth, allowing to the proposition of algorithms to automatically generate dynamic models for any number of links considered in discrete approximation.

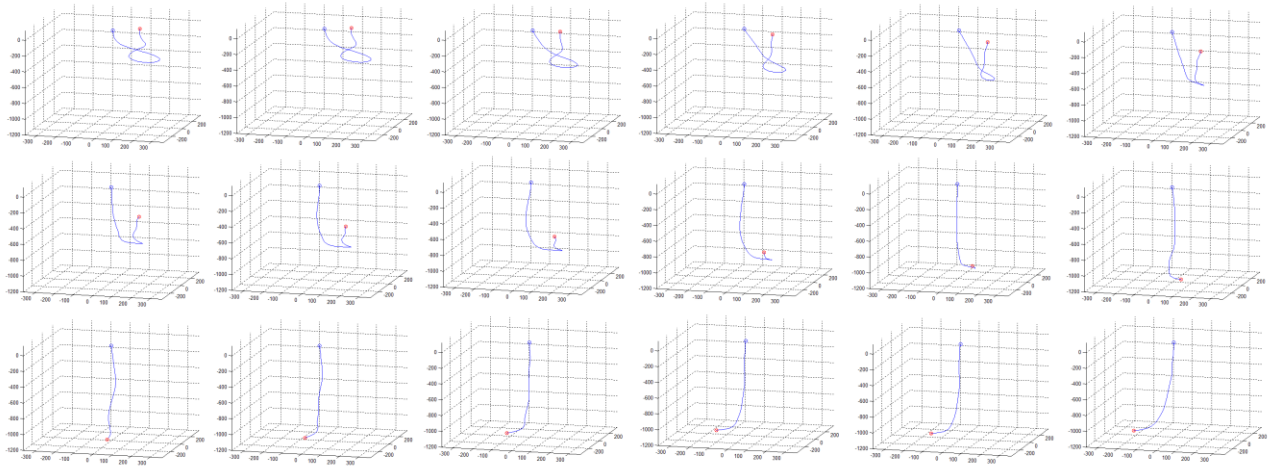

Fig. 5. Free fall simulation, underwater, frames every 2 seconds.

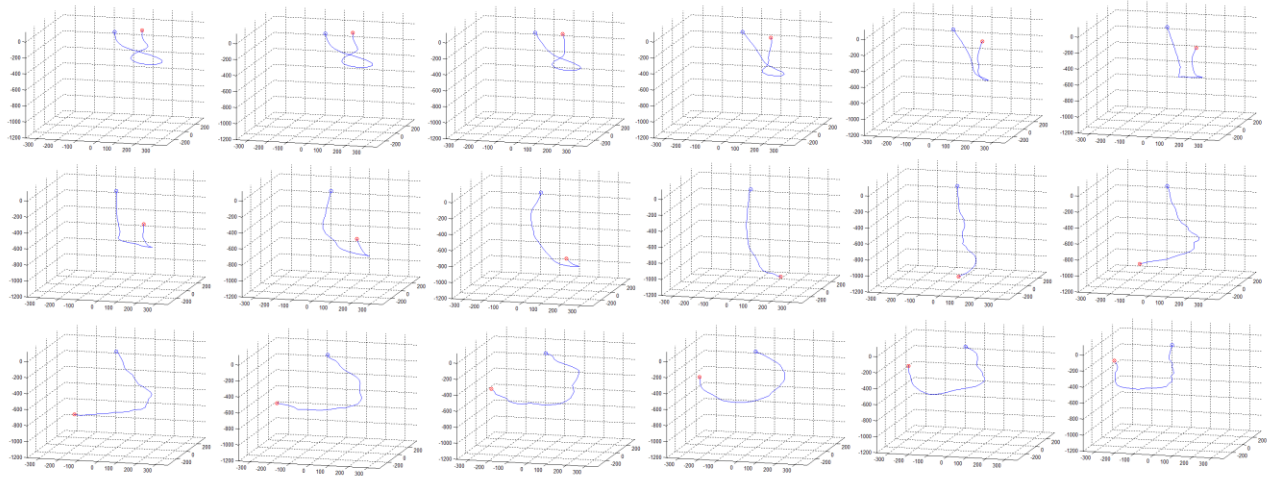

Fig. 6. Free fall simulation, out of water, frames every 2 seconds.

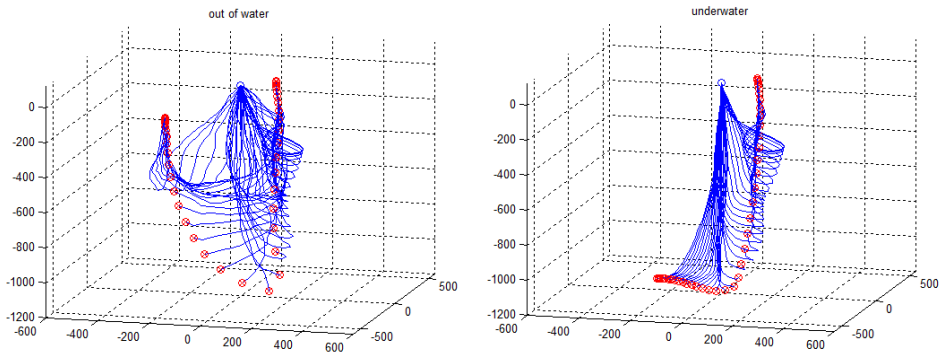

Fig. 7. Free fall simulations, out of water and underwater, from zero to 40 *s*, frames every 1 *s*.

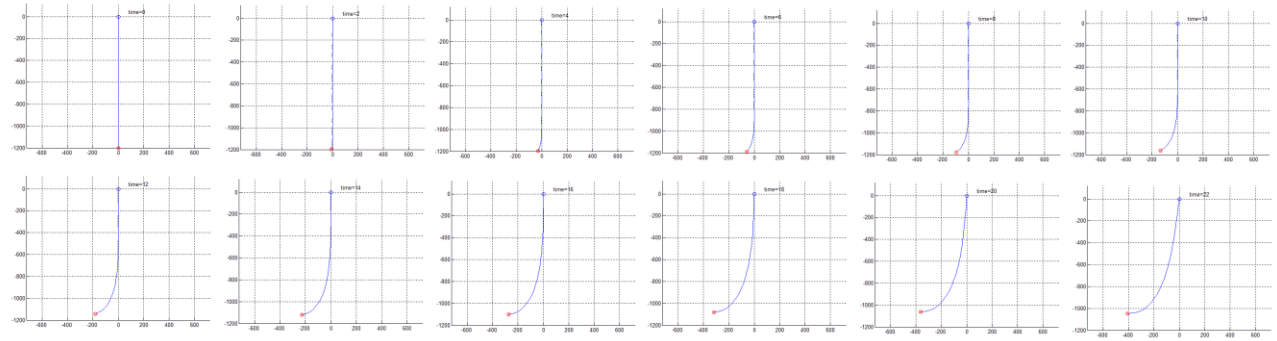

Fig. 8. Cable under the action of underwater current, from 0 to 22 *s*, frames every 2 *s*.

The simulations were chosen in order to know a priori what should be the dynamic behavior of the cable and, in all cases the results were in agreement with the physically expected. Torsion motion was considered in cable modeling

because in future applications, there is an interest in having a ROV as a cable terminal load. In this case, forces applied to the ROV can generate torsion in the cable. It has been specially developed software that performs three-dimensional animations of the cable's spatial configuration, for better visualization and analysis of simulation results. Three-dimensional animations allowed us to identify a great sense of physical reality. Increasing the number of links implies a better discrete approximation of the continuous flexibility. It was observed that over forty links the discrete model closely matches the continuous flexibility. In future works it is planned to build an experimental support sensed by digital cameras to validate simulations and physical parameters identification strategies.

REFERENCES

Breukels, J. and Ockels, W. J. A multi-body dynamics approach to a cable simulation for kites. Proceedings of the IASTED Asian Conference on Modelling and Simulation. Beijing, CHINA, October, 2007.

Buckam, B., Driscoll, F.R. and Meyer, N. Development of a Finite Element Cable Model for Use in Low-Tension Dynamics Simulation. J. Appl. Mech, -Volume 71, Issue 4, 476, July 2004.

Dreyer T.P. and Van Vuuren, J. H. A comparison between continuous and discrete modelling of cables with bending stiffness. Applied Mathematical Modelling. 23 (1999), pgs 527-541.

Gobat, J. I. The Dynamics of Geometrically Compliant Mooring Systems. PhD Thesis, Massachusetts Institute of Technology, 2000.

Gomes, S. C. P., Rosa, V. S. and Albertini, B. C. Active control to flexible manipulators. IEEE/ASME Trans. on Mechatronics, vol. 11, no. 1, pp. 75–83, USA, 2006.

Gomes, S. C. P., Zanela, B. E. and Pereira, A. E. L. *Automatic generation of dynamic models of cables*. http://dx.doi.org/10.1016/j.oceaneng.2016.05.041. Ocean Engineering, volume 121, pgs 559–571, (2016).

Gosling, P.D. and Korban, F.A. A bendable finite element for the analysis of flexible cable structures. Finite Elements in Analysis and Design. 38: 45-63, 2001.

Hall, M. and Goupee, A. Validation of a lumped-mass mooring line model with DeepCwind semisubmersible model test data. Ocean Engineering, 104, 590–603, 2015.

Hover, F.S., Grosenbaugh, M.A. and Triantafyllou, M.S. Calculation of dynamic motions and tensions in towed underwater cables. IEEE Journal of Oceanic Engineering, Vol. 19, No. 3, July 1994.

Lacarbonara, W. and Pacitti, A. Nonlinear Modeling of Cables with Flexural Stiffness. Mathematical Problems in Engineering, 2008.

Lee, C., Hong, S., Kim, H. and Kim, S. A comparative study on effective dynamic modeling methods for flexible pipe. Journal of Mechanical Science and Technology 29 (7) 2721~2727, 2015.

Matulea, I.C., Nastase, A., Talmaciu, N., Slamnoiu, G. and Coelho, A. M. G. On the equilibrium configuration of mooring and towing cables. Applied Ocean Research, 30, 81-91, 2008.

Matulea, I., Ştefan, D., Vladescu, D., Barbu, C. and Coelho, A. M. G. A Novel Numerical Approach to the Dynamics Analysis of Marine Cables. International Journal of Applied Science and Technology, Vol. 4 No. 2; March 2014.

Pereira, A. E. L., Gomes, S. C. P. and Bortoli, A. L. A new formalism for the dynamic modeling of cables. Mathematical and Computer Modeling of Dynamical Systems, v. 1, p. 1-14, 2012.

Raman-Nair, W. and Williams, C.D. Vortex-Induced Response of a Long Flexible Marine Riser in a Shear Current. International Symposium on Technology of Ultra Deep Ocean Engineering. Feb 1-2, Tokyo, Japan, 2005.

Srinil, N., Rega, G. and Chucheepsakul, S. Two to one resonant multi-modal dynamics of horizontal/inclined cables. Part I: Theoretical formulation and model validation. Nonlinear Dyn. 48:231-252, 2007.

Srivastava , V. K., Sanyasiraju, Y. and Tamsir M.. Dynamic behavior of underwater towed-cable in linear profile. International Journal of Scientific & Engineering Research Volume 2, Issue 7, July-2011.

Sun , F.J.; Zhu, Z.H and LaRosa, M. Dynamic modeling of cable towed body using nodal position finite element method. Ocean Engineering 38, 529–540, 2011.

Zhu, K.-Q., Zhu, H.-Y., Zhang,Y.-S. and Gao, J. A multi-body space-coupled motion simulation for a deep-sea tethered remotely operated vehicle. Journal of Hydrodinamic. 20(2):210-215, 2008.

Yoon, J.W., Park, T.W. e Yim, H.J. Fatigue life prediction of a cable harness in an industrial robot using dynamic simulation. Journal of mechanical science and technology. ISSN 1738-494X, Vol.22, nº 3, pp. 484-489, 2008.

Wang, F., Huang, G. and Deng, D. Steady State Analysis of Towed Marine Cables. J. Shanghai Jiaotong Univ. (Sci), 13(2):239-244, 2008.

Wang, P.H., Fung, R.F. and Lee, M.J. Finite Element analysis of a three-dimensional underwater cable with time-dependent length. Journal of Sound Vibration. Volume 209, Issue 2, Pages 223-249, January 1998.

Wen-ShouZhang and Dong-Dong Li. Active control of axial dynamic response of deepwater risers with Linear Quadratic Gaussian controllers. Ocean Engineering 109, 320–329, 2015.

RESPONSIBILITY NOTICE

The author(s) is (are) the only responsible for the material included in this paper.